論　文

Numerical Analysis of Viscoelastic Flow Based on FENE-P Model using High-order Accuracy Finite Difference Method

Yonghua CHENG[*1], Mizue MUNEKATA[*2],

Kazuyoshi MATSUZAKI[*2] and Hideki OHBA[*3]

1. Introduction

It has been known for almost half a century that, solutions of a slight additive of long-chain high-molecular-weight polymer to a turbulent Newtonian solvent can cause significant friction drag reduction in pipe or channel flow. This discovery was first recognized by Toms and termed Toms phenomenon[1]. It means, with the dilute polymer solutions, a lower pressure gradient is needed to maintain a higher flow rate. This effect is considered very usefully and effectively in the fluid transportation engineering area. A striking feature of Toms phenomenon is that it can occur even at very low concentrations and attain up to 70% drag reduction.

A vast of investigations has been encouraged on studies about the drag reduction mechanism of Toms phenomenon. These can be roughly divided into three approaches[2]. The first of them is concentrating on the behavior of polymer molecules in various model flows. The second is including mainly the effects of polymers on the flow turbulent statistics, with examining the mean velocity profile, velocity fluctuation and so on. The last one is conducted to the study in coherent turbulent structure with polymer additives. The several conclusions have been made clear[3]-[5].

The available experimental information would be used in interpreting and developing theoretical ideas for the mechanism of drag reduction. The basic explanations for the Toms phenomenon were proposed as[6] (1) Effective slip (increasing of buffer layer close to wall); (2) Anisotropic viscosity (for example elongation viscosity); and (3) Visco-elasticity. However, why and how the factors above can act between the polymer and turbulent flow, further induce reduction of friction drag? It might be conducted that, a viscoelastic flows, with both properties of a viscous liquid and an elastic solid, possess a partial memory characterized by a relaxation time. This relaxational effect (elastic memory) enhances macromolecular resistance and then causes the drag reduction[6]. In other way, it was proposed that, the change of turbulent structure is based on the change of redistribution in pressure-strain correlation near the vicinity of wall[5]. It is hard to capture the details containing such complex properties because the direct experiment is so difficult.

With the high speed development in computer technology, computational fluid dynamics (CFD) has become more important and direct numerical simulation (DNS) responding to turbulent flows could be possible[7]. It has also been desired to

perform the numerical simulation to the viscoelastic flow and further, to realize the mechanism of drag reduction in polymer additives. In the non-Newtonian flow computations, the constitutive equation modeling non-Newtonian characteristics is necessary and it has been considered difficult to get a stable computation[8]. Nevertheless, several applications of numerical simulation schemes to viscoelastic flow have been conducted. Den Toonder et al.[9] investigated a pipe turbulent flow by using an elongation viscosity model comparing with the Maxwell model to describe the effect of polymers on a pipe flow and evaluated that preferably anisotropic enhanced extensional viscosity of a polymer solution act a critical role in drag reduction. More recently, Kajisima et al.[10] presented a bead-spring-dashpot model applying to a channel flow and considered with this approach, the micro motions of molecules could be followed. But a relatively more parameters must be assumed and it is hard to control. Since FENE-P (finite extension nonlinear elastic-Peterlin) model has been introduced[11], the numerical simulation of polymer molecule becomes more vigorous. Based on this model, Massah at el.[12] focused on the behavior of polymer-molecule and calculated the additional stress from the constitutive equation, resulted that increasing of the eddy structure scale near the wall leads increasing buffer layer border and then damps the friction drag. Chiba et al.[13] applied Brownian dynamics simulation of FENE modeling rheological behaviors of dilute polymer solution, and obtained the distributions about relaxation time and other model parameters. But in the researches mentioned above, one-way influence in polymer from the turbulent flow are considered, and modification of turbulent structure from polymer is not touched. Surehkmar et al.[14] addressed FENE-P model to the turbulent channel flow by means of DNS method. The onset of drag reduction, general turbulent statistics, the streak structure and energy spectrum are computed and compared between Newtonian and non-Newtonian flows. However, in order to ascertain a stable numerical integration of constitutive equation, an artificial stress diffusive term was conducted additionally. The explanation about this artificial diffusive is too lacking. Besides, since DNS method is limited with its periodic boundary condition, it is hard to implement complex flow field computations to solve application problems in current fluid engineering area.

This work is to develop the FENE-P model by using a high-order accuracy finite difference method[15]. We performed an effective numerical simulation scheme with the upwind difference method, to solve the polymer additive solution in the channel flow. In constitutive equation, the 3rd-order accurate upwind difference scheme was applied and steady resolution was achieved.

2. Mechanical model of polymer molecules

An actual polymer molecule is an extremely complex mechanical system differing from the lower molecules with great diversity in structure, molecular weight distribution and large number of internal degrees of freedom. Investigating the detailed motions of this complicated system and their properties would be prohibitively difficult. It is considerably necessary to use simplified models to represent molecules in order to minimize the mathematical complications. The crude "dumbbell" chain models were introduced earliest, in which bead-rod and bead-spring chain were used to represent chainlike macromolecules[11]. Although more complex models accounting chain branching or other effects were developed later, it was necessary to use considerably simpler models in order to do the mathematics and numerical work for obtaining the useful results with description of macromolecular configurations and the associated rheological properties. The simpler models have contributed greatly to our understanding of polymer rheology and fluid dynamics.

Let us get a view in the simpler and useful chain models in fluid dynamics. Fig. 1 shows a freely jointed bead-rod chain model formed from N beads of mass m and friction coefficient ζ connected by
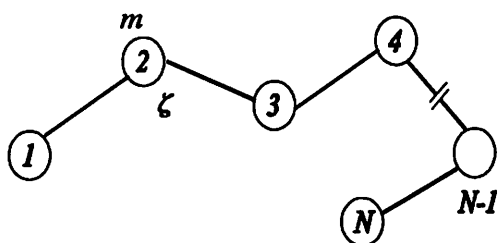
Fig. 1   The freely jointed bead-rod chain model

Fig. 3   The elastic dumbbell model

$N-1$ rigid, massless rods. This model possesses a number of important features in formulating a kinetic theory for rheological behavior of a polymeric liquid. It has a large number of internal degrees of freedom ; it can be oriented, stretched, and deformed ; it has a constant contour length. The second chain model is shown in Fig. 2 named freely jointed bead-spring chain with spring connections instead of rods. Each bead is presumed to experience a drag force as it moves through the flow field, and the drag could be described by using Stokes' law. This model is considerably simpler to handle and more flexible to implement than the bead-rod chain model, because it exists no internal constraints and contains many kinds of elastic characteristic by choice of the spring force law.

One considers the very simplified models that N is set equal to 2, named the dumbbell models. Fig. 3 shows an elastic dumbbell model. This dumbbell model is only very crude representations of polymer molecules. It certainly does not have enough internal degrees of freedom. However, by using this dumbbell model, it is possible to perform kinetic theory derivations and calculations for rheological properties, then further to get constitutive equations, and finally to solve some useful
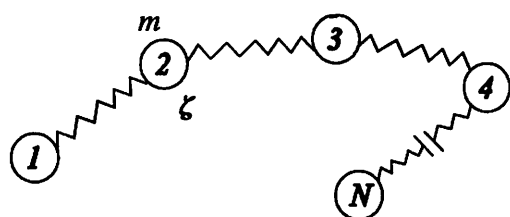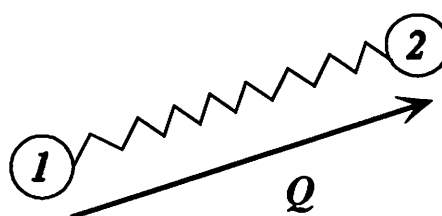
flow problems. All of these can be done with a limited amount of mathematical effort. In other words, we can control the entire procedure from molecular model to fluid dynamics. In turn, the analytical results for dumbbell models can be used also to check computational simulation procedures in molecular dynamics and Brownian dynamics.

All of above, the elastic dumbbell models have been proven to be particularly popular in developing an elementary between macromolecular motions and rheological phenomena. This model is orientable and stretchable, and these two properties are essential for the qualitative description of steady-state rheological properties. On the other hand, the spring force law can enable us to obtain a wide analytical solution to various polymer fluid dynamics problems.

By using an elastic dumbbell model, the connector force between bead-to-bead is, in generally, given by following law.

$$F^{(c)} = f(Q^2)Q \tag{1}$$

Here, f is a scale function of $Q^2 = Q \cdot Q$, while $Q = r_2 - r_1$ is the bead-to-bead (or end-to-end) vector, r_1 and r_2 are the bead position vectors. Based on the choice of the spring force law, we can get many kinds of elastic dumbbell models as mentioned above. The most simplified model is named Hookean-dumbbell model, in which $f(Q^2) = H$ and H is a spring constant independent of the bead-to-bead vector. As we can image, the distinct disadvantage of Hookean dumbbell model is that spring can be stretched out to any length infinitely. It predicts a constant value for steady shear viscosity and infinite elongational viscosity at a finite elon-

Fig. 2   The freely jointed bead-spring chain model

gation rate. So the Hookean dumbbell model is limited in application. One of the improved models from Hookean model is named FENE model by introducing a nonlinear connector force and having a configuration-dependent "spring constant" given by

$$f(Q^2) = \frac{H}{1 - Q^2/Q_0^2} \qquad (2)$$

Where Q_0 is the maximum extension $(Q \leq Q_0)$. An upper limited length Q_0 constraints these finitely extendable nonlinear elastic connectors.

3. Governing equations

3.1 Basic equations

The basic equations describing such these incompressible flows are given by the momentum equation and continuity equation.

$$\rho \frac{\partial V}{\partial t} + \rho V \cdot \nabla V = -\nabla p + \nabla \cdot \tau \qquad (3)$$

$$\nabla \cdot V = 0 \qquad (4)$$

In these equations, V is the velocity vector, ρ is the density of solution, p is the pressure and τ is the deviatoric stress tensor. This stress tensor τ is given by the sum of two terms, which first term is due to the Newtonian solvent and the second term can be considered as the polymer contribution

$$\tau = \tau_N + \tau_P \qquad (5)$$

For Newtonian contribution τ_N, viscous constitutive equation is well known as

$$\tau_N = 2\eta_s D \qquad (6)$$

Here D is the rate-of-strain tensor, which is the symmertric part of the velocity gradient $D = (\nabla V + \nabla V^T)/2$, and η_s is the solvent viscosity. For polymer contribution τ_P, a constitutive equation depending on the elastic dumbbell model must be supplied. We discuss it in the next section.

3.2 Constitutive equations

In non-Newtonian flow simulations, the development of a constitutive equation for the stress ten-

sor, in general, is satisfied in following ways: (1) The equation is chosen empirically to fit experimental data as well as possible. (2) Continuum mechanics can be used to generate "reduced equations" appropriate for specific classes of flows. (3) Molecular theory can lead to a constitutive equation in terms of parameters of the mechanical model. Basing on these rules, in this work, because the contribution to the stress tensor is realized as elastic dumbbells, we can develop the constutive equation from kinetic theory with FENE -P model. As discussed before, we choose this model because it contains the basic characteristics of streching, orientation, and finite extensibility seen in polymer molecules, yet it has relatively simple mathmatical expressions.

In this method, τ_P value can be derived from two terms of averages in the momentum fluxes genarated by spring tension (the first term of following equation) and bead motion (the second term)

$$\tau_p = -n < QF^{(c)} > + nKT\delta \qquad (7)$$

Here K is Boltzmann's constant and T is the absolute temperature, while n is the number of polymer molecules in a unit of volume and δ is unit tensor. The angular brackets $< >$ denote a configuration-space average. By substituting connector force of the FENE model with equation (1) and (2), we can get expression.

$$\tau_p = -n \left\langle H \frac{QQ}{1 - Q^2/Q_0^2} \right\rangle + nKT\delta \qquad (8)$$

However, this equation can not be used directively to get a constitutive equation because the configuration-space average value can not be easily evaluated by ensemble average approach. Therefore, we must approximate the average value with following way which is first suggested by Peterlin[16] and then be renamed FENE model to FENE-P model

$$\left\langle \frac{QQ}{1 - Q^2/Q_0^2} \right\rangle \approx \frac{\varepsilon \langle QQ \rangle}{1 - \langle Q^2/Q_0^2 \rangle} \qquad (9)$$

where ε is a constant which improve the approxi-

mation. Thus, the polymer contribution to the stress tensor in equation (8) can be alternatively expressed by using $C = \langle QQ \rangle (H/KT)$. This C is defined as a comformation tensor and it is symmetric and positive definitely.

$$\tau_p = -nKT\left(\frac{\varepsilon C}{1-r^2/L^2}-\delta\right) \qquad (10)$$

Where

$$r^2 = Q^2H/KT = trace(C) = C_{11} + C_{22} + C_{33}$$

is dimensionless and explanized as a ratio of the elastic spring energy to the thermal energy. L is the maximum value of $r (r \leq L)$. To determine the constant ε, we illustrate the process of a equilibrium unit isotropic tensor $C = \delta$. At this process the shear stress contribution τ_P should be zero. So we can easily get value $\varepsilon = 1 - 3/L^2$ with $C = \delta$, $\tau_P = 0$ from equation (10). The shear stress τ_P can be then written to :

$$\tau_p = -nKT(f(r^2)C-\delta) \qquad (11)$$

and

$$f(r^2) = \frac{L^2-3}{L^2-r^2} \qquad (12)$$

Bird et al. also introduced another stress tensor expression which named Giesekus form by deriving from "diffusion equation" (Ref. [11], Page 88).

$$\tau_P = \frac{n\zeta}{4}\langle QQ \rangle_{(1)} \qquad (13)$$

Here friction coefficient ζ definitely connected with the relaxation time λ, which is defined as relation $\lambda = \zeta/4H$ and characterize a partial memory of viscoelastic solution[8),11)]. $\alpha_{(1)}$ denotes the upper-convected derivative for arbitrary tensor α expressed as

$$\alpha_{(1)} \equiv \frac{\partial}{\partial t}\alpha + V \cdot \nabla \alpha - (\nabla V)^T \cdot \alpha - \alpha \cdot \nabla V \qquad (14)$$

We can alternatively express equation (13) as following form by introducing λ and C.

$$\tau_P = nKT\lambda C_{(1)} \qquad (15)$$

Comparing equation (11) and (15), we can get following constitutive equation to calculate conformation tensor C.

$$\frac{\partial}{\partial t}C + V \cdot \nabla C - (\nabla V)^T \cdot C - C \cdot \nabla V = -\frac{f(r^2)C-\delta}{\lambda} \qquad (16)$$

In order to evaluate τ_P value from equation (11), it is necessary to consider eliminating nKT. The upper-convected Maxwell model could be applied[17)].

$$\lambda\tau_{P(1)} + \tau_P = 2\eta_P D \qquad (17)$$

Where η_P is a polymer viscosity named from a polymeric contribution to the total shear viscosity. By substituting equation (11) and (15) into the first term and the second term in equation (17), respectively, we can be given

$$-\lambda nKT\{f(r^2)C_{(1)}-\delta_{(1)}\} + \lambda nKTC_{(1)} = 2\eta_P D \qquad (18)$$

Since this equation must also be satisfied in the equilibrium unit isotropic state with $C = \delta$ and $f(r^2) = 1$ conditions, so following relation can be obtained.

$$\lambda nKT\delta_{(1)} = 2\eta_P D \qquad (19)$$

Then because of $\delta_{(1)} = -2D^{17)}$, relation $nKT = -\eta_s/\lambda$ must be derived. Thus equation (11) becomes

$$\tau_P = \frac{\eta_P}{\lambda}\{f(r^2)C-\delta\} \qquad (20)$$

All of above, equation (1), (2), (16) and (20) constitute the governing equations for the viscoelastic flow and subsequently can be solved numerically.

4. Numerical procedure

The flow geometry and the coordinate system are shown in Fig. 4. The simulation is carried out in a domain of $6.4h \times 2h \times 3.2h$ in the mean streamwise x, the wall-normal y and the spanwise z directions, respectively, with h channel half-width. A constant pressure drop gradient along with the channel streamwise direction is imposed externally. It is customary to make the governing
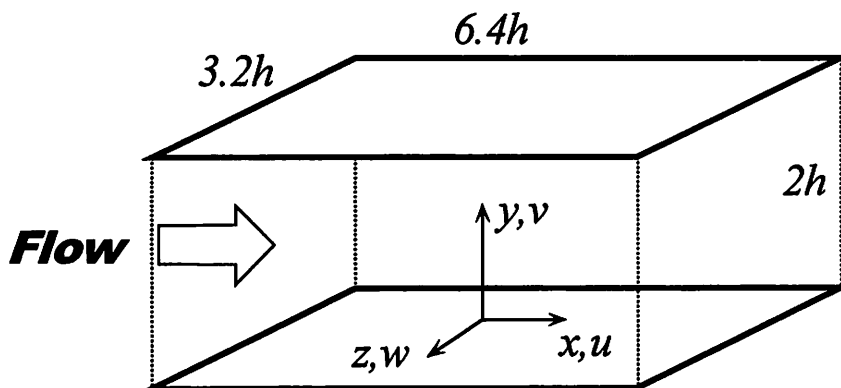
Fig. 4　The channel flow and coordinate

equations dimensionless by using the friction velocity u_τ, channel half-width h and kinetic viscosity ν. In the viscoelastic solution, however, a zero-shear kinematic diffusivity ν_0 is denoted as a scale parameter instead of ν. This zero-shear kinematic diffusivity is defined by $\nu_0 = \eta_0/\rho$, with total zero-shear viscosity η_0 and density ρ. The zero-shear viscosity includes solvent viscosity and polymer viscosity $\eta_0 = \eta_s + \eta_P$. The polymer shear stress τ_P is made dimensionless with $\eta_P u_\tau^2/\nu_0$. The basic equation (3) then can be written in following dimensionless expression

$$\frac{\partial V^*}{\partial t^*} + V^* \cdot \nabla V^* = -\nabla p^* + \frac{\eta_s}{\rho\nu_0}\frac{\nu_0}{u_\tau h}\nabla^2 V^* + \frac{\eta_P}{\rho\nu_0}\nabla \cdot \tau_P^*$$

Symbol * indicate the dimensionless quantities. Let us eliminate symbol * to simply express equations in later discussion. We denote Reynolds number as $\mathrm{Re} = u_\tau h/\nu_0$ and the ratio parameter of solvent viscosity η_s to total zero-shear viscosity η_0 as $\beta = \eta_s/\eta_0$. Then the above equation can be expressed by following equation without * symbol.

$$\frac{\partial V}{\partial t} + V \cdot \nabla V = -\nabla p + \beta\frac{1}{\mathrm{Re}}\nabla^2 V + (1-\beta)\nabla \cdot \tau_P \quad (21)$$

With the same approach, equation (16) and (20) can also be rewritten in dimensionless expressions by

$$\frac{\partial}{\partial t}C + V \cdot \nabla C - (\nabla V)^T \cdot C - C \cdot \nabla V = -\frac{f(r^2)C - \delta}{We/\mathrm{Re}} \quad (22)$$

$$\tau_P = \frac{f(r^2)C - \delta}{We} \quad (23)$$

Where $We = \lambda u_\tau^2/\nu_0$ is the Weissenberg number defined as the product of the polymer relaxation time and a characteristic shear rate.

To solve the basic equation (21), the high-order accuracy finite difference method[15] based on the fractional step scheme[18] is employed, and this scheme is expressed by

$$\frac{\hat{V} - V^n}{\Delta t} = \frac{1}{12}(23A^n - 16A^{n-1} + 5A^{n-2}) + \frac{\beta}{\mathrm{Re}}\nabla^2(\hat{V} + V^n)$$

$$\nabla^2 p^{n+1} = \frac{1}{\Delta t}\nabla \cdot \hat{V}$$

$$\frac{V^{n+1} - \hat{V}}{\Delta t} = -\nabla p \quad (24)$$

Where A represents the sum of the convective term and polymer stress contribution term: $A = -V \cdot \nabla V + (1-\beta)\nabla \cdot \tau_P$. The time marching method with the 3rd-order Admas-Bashforth method for A term and the Crank-Nicolson method for viscous term is performed here. The spatial derivatives are approximated using the 4th-oredr centered finite difference for Poisson equation, the 6th-oreder centered finite difference for the viscous term and the 5th-order upwind finite difference scheme for the convective terms. The 5th-order upwind finite difference scheme is given from Rai et al.[19] by

$$\left(u\frac{du}{dx}\right)_i = u_i\frac{u_{i+3} - 9u_{i+2} + 45u_{i+1} - 45u_{i-1} + 9u_{i-2} - u_{i-3}}{60\Delta x} +$$

$$|u_i|\frac{-u_{i+3} + 6u_{i+2} - 15u_{i+1} + 20u_i - 15u_{i-1} + 6u_{i-2} - u_{i-3}}{60\Delta x} \quad (25)$$

To solve the constitutive equation (22), the 2nd -order accurate Admas-Bashforth explicit method is applied.

$$C^{n+1} = C^n + \frac{\Delta t}{2}(3B^n - B^{n-1}) \qquad (26)$$

Here

$$B = \frac{\partial C}{\partial t} = -V \cdot \nabla C + (\nabla V)^T \cdot C + C \cdot \nabla V - \frac{f(r^2)C - \delta}{We/\mathrm{Re}}$$

To ascertain a stable numerical integration of the evolution equations, the 3rd-order accurate upwind finite difference method[20] is considered in spatial derivative of $V \cdot \nabla C$ term.

$$\left(u\frac{dc}{dx}\right)_i = u_i \frac{-c_{i+2} + 8c_{i+1} - 8c_{i-1} + c_{i-2}}{12\Delta x} + $$
$$|u_i| \frac{c_{i+2} - 4c_{i+1} + 6c_i - 4c_{i-1} + c_{i-2}}{4\Delta x} \qquad (27)$$

Other spatial derivatives are approximated using 4th-order accurate centered finite difference method.

5. Computational conditions

The periodic boundary conditions are used for all of the computational variables in the streamwise x and spanwis z directions because fully developed turbulent channel flow is homogeneous in those directions and the computational domain is chosen to include the largest eddies in the flow. In y direction, the non-slip boundary conditions for velocity and the Neumann boundary conditions for pressure are applied on the channel walls. For the conformation tensor, the boundary conditions are supplied by integrating the constitutive equation directly as the solid boundaries.

$$(C^{n+1})_{wall} = (C^n)_{wall} + \Delta t \cdot B^n \qquad (28)$$

With

$$(V)_{wall} = 0; \quad \left(\frac{\partial}{\partial x}\right)_{wall} = 0; \quad \left(\frac{\partial}{\partial z}\right)_{wall} = 0$$

Since high order accurate finite difference is used, a seven-point stencil for 5th-order upwind scheme

and 6th-order centered scheme is conducted and two fictitious grid points outside of a boundary are required for velocity boundary condition. In this work, the principal of mirror image is applied as a special treatment on the wall boundaries.

As initial conditions, the velocity and pressure are considered using the database corresponding to the fully turbulent Newtonian channel flow. For the conformation tensor, Following Sureshkumar at el.[14], using the average velocity $U(y)$ computed by the initial velocity, the assumption of a one -directional shear flow (x-direction) with the velocity profile given by $U(y)$ is introduced. Based on the constitutive equation (22), with assumptions: $\partial/\partial t = 0$, $\partial/\partial x = 0$, $\partial/\partial z = 0$, $v = w = 0$, the conformation tensor components can be evaluated.

$$C^0{}_{11} = \frac{1}{F(y)}\left[1 + \frac{2We^2}{F^2(y)}\left(\frac{dU}{dy}\right)^2\right];$$
$$C^0{}_{22} = C^0{}_{33} = \frac{1}{F(y)};$$
$$C^0{}_{12} = \frac{We}{F^2(y)}\frac{dU}{dy};$$
$$C^0{}_{13} = C^0{}_{23} = 0 \qquad (29)$$

Here,

$$F(y) = \frac{\sqrt{3}\,\Omega(y)}{2\sinh(\phi/3)}$$

With

$$\Omega(y) = \frac{\sqrt{2}}{L}We\frac{dU}{dy},$$
$$\phi = \sinh^{-1}(3\sqrt{3}/2)$$

In order to conduct relations of $F(y)$, $\Omega(y)$ and ϕ, $f(r^2)$ function is used. This procedure yields the conformation tensor components evaluated using the mean shear flow assumption.

The computation is carried out with $64 \times 65 \times 64$ grid points in x, y and z directions, respectively. The grid spacing in the streamwise and spanwise directions are equal spacing with the grid resolution respectively $\Delta x^+ = 18$ and $\Delta z^+ = 9$ in wall units. Non-uniform meshes are used in the wall-normal direction generating with tanh function distribution and $\Delta y^+ = 0.45 - 13.9$ grid spacing. We choose the

Reynolds number Re as 180, the weissenberg number We as 50, and L value as 10. This Reynolds number corresponds to about 3300 mean Reynolds number based on mean velocity. It has been proven that, experimentally, the drag reduction in dilute polymer solution had been observed at higher Reynolds number corresponding to 8900 or higher. In order to compensate this lower Reynolds number we applied, the ratio value β is set to 0.9, to simulate a more elastic behavior of flow to capture the drag reduction effectively.

6. Results and discussions

6.1 Mean velocity profile

In Fig. 5 the non-dimensional mean velocity profiles are illustrated as a function of wall distance scaled by $y^+=yu_\tau/\nu$ for Newtonian flow and $y^+=yu_\tau/\nu_0$ for viscoelastic flow. The functions, given by $u^+=y^+$ (with $y^+<5$) and $u^+=2.5\ln(y^+)+5.5$ (with $y^+>30$), are generally believed to describe the mean streamwise velocity profile of the Newtonian turbulent flow. The regions $y^+<5$, $5<y^+<30$ and $y^+>30$ are called the viscous sublayer, buffer layer and logarithmic layer, respectively. We would like to indicate that, in this computation, the Newtonian data do not follow the logarithmic law well, this is because the grid number we used here is much fewer than those of Kim et al.[7]. In this Fig., it can be seen that, the viscoelastic velocity profile obtained by FENE-P
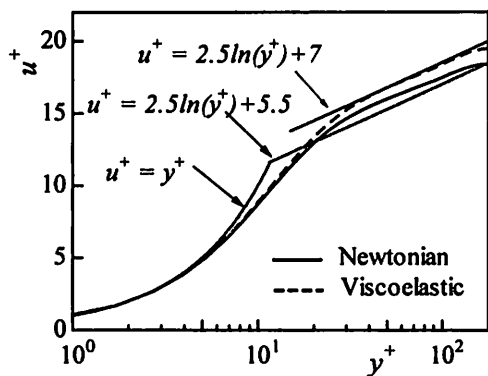
model almost completely follows the Newtonian data within viscous sublayer $y^+<5$. In the logarithmic layer, however, the viscoelastic profile is shifted upward with an approximate relation $u^+=2.5\ln(y^+)+7$, comparing to the Newtonian flow case. This absolutely confirms an increment of flow rate and reduction of friction drag by polymer additive. Since the intercept distance between the sublayer and logarithmic layer is increased for the viscoelastic flow (about $y^+\approx 5\sim40$) comparing to Newtonian case ($y^+\approx 5\sim30$), the buffer layer is considered to be extended in the case of viscoelastic flow. It has been interpreted, the effect of the polymer additive is to thicken the buffer layer so that a mean velocity arises in the center of channel for same wall stress. In other words, a lower wall stress is required for the same maximum velocity and so drag reduction occurs.

6.2 Velocity fluctuations

Fig. 6 shows the non-dimensional root mean square (r.m.s) profiles of velocity fluctuations in x, y and z direction components against y^+ in the wall region. As can be seen, there is not any significant difference between two flow cases in the center of channel. However, in the buffer layer, the viscoelastic r.m.s profile is increased for the streamwise component, and decreased for both of the wall-normal and spanwise components as compared to the Newtonian results. These changes in turbulence intensities have also been experimentally confirmed. It demonstrates that
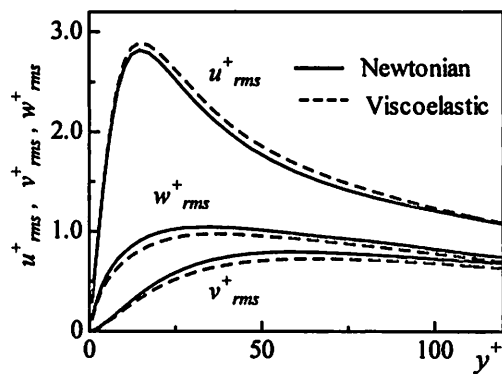

Fig. 5 The mean velocity profile

Fig. 6 Root-square of velocity fluctuation

the turbulence structure is not generally suppressed by introduce of polymer additive. In fact, the turbulent structure is modified due to the resistance of polymer molecule in the wall region. Unfortunately, in this work, the location shift of maximum r.m.s value in x component is not shown clearly. This may be attributed to the fewer grid number, as same as discussed in the Newtonian mean velocity distribution, which does not completely follow the logarithmic law.

6.3 Shear stress

Fig. 7 illustrates the Reynolds shear stress (turbulent stress) $-\overline{u'^+v'^+}$ and sum of shear stress contributed from both of Reynolds shear stress component and purely viscous component : $-\overline{u'^+v'^+}+dU/dy^+$ for two flow cases as a function of y/h. The symmetry of these profiles about the channel centerline demonstrates that the total averaging time and statistical sample are adequate. In the fully developed turbulent channel flow, the total of the shear stress would be distributed as a straight line $1-y/h$ to balance the downstream mean pressure gradient when the flow reaches an equilibrium state. As shown from this Fig., in Newtonian fluid, the sum shear stress decreases almost following linear line $1-y/h$ and shows that the average turbulent shear stress profile has attained the equilibrium shape. Nevertheless, for viscoelastic case, it was found clearly, Reynolds stress $-\overline{u'^+v'^+}$ is suppressed comparing to Newtonian case because of polymer additive.
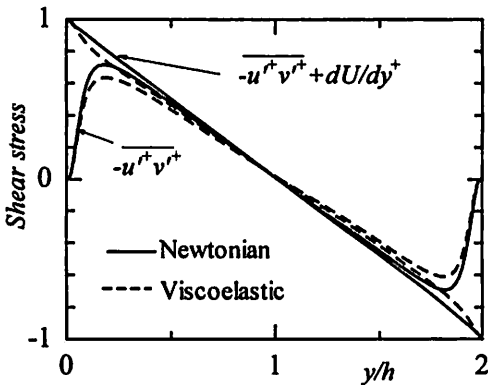
Therefore, the sum stress does not add up to a linear dependence on y/h. This fact has been also observed in experiments and attributed to the neglected viscoelastic contribution in this sum stress. Accurately, in the viscoelastic flow, the total shear stress has to be decomposed into three contributions from Reynolds shear stress S_R, purely viscous S_V and viscoelastic force S_P, respectively. For fully developed viscoelastic turbulent flow, the total of the shear stress must obey the balance :

$$S_{total}=S_R+S_V+S_P=1-y/h \qquad (30)$$

This viscoelastic contribution S_P can be evaluated by the component value τ_{P12} of stress tensor τ_P. Based on the governing equation (21), this balance relation thus is given by

$$-\overline{u'^+v'^+}+\beta\frac{dU}{dy^+}+(1-\beta)\tau_{P12}=1-y/h \qquad (31)$$

Fig. 8 shows these three contributions and total shear stress of viscoelastic flow. It has been seen, the profile of the total shear stress decreases nearly linearly with y/h. The viscoelastic contribution S_P to total shear stress is a small positive value and completely compensated the deficient observed in Fig. 7. It also implies an equilibrium state is achieved for viscoelastic turbulent fluid flow.

6.4 Vorticity fluctuations

The vorticity are defined by

$$\omega_x=\frac{\partial v}{\partial z}-\frac{\partial w}{\partial y}; \quad \omega_y=\frac{\partial w}{\partial x}-\frac{\partial u}{\partial z}; \quad \omega_z=\frac{\partial u}{\partial y}-\frac{\partial v}{\partial x} \qquad (32)$$
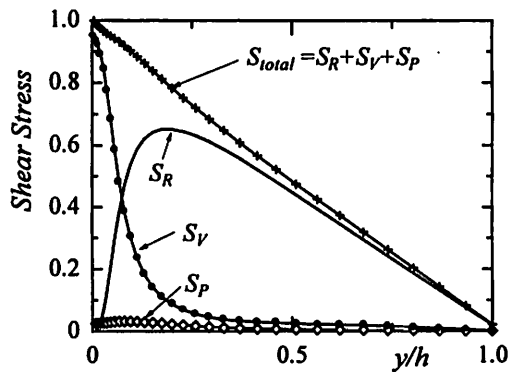

Fig. 7   The shear stress of two flows

Fig. 8   The shear stress of viscoelastic flow

The r.m.s profiles of vorticity fluctuations normal-ized by $u^2{}_\tau/\nu$ are illustrated in Fig. 9 as a function of y/h. It has been known, $\omega^+{}_{z,rms}$ and $\omega^+{}_{x,rms}$ components attain their maximums at the wall, away from the wall, the three components of vor-ticity fluctuations become small and identical, in spite of larger differences near the wall.   There are almost no differences of the vorticity fluctuations between Newtonian and viscoelastic flows in the wall-normal and spanwise components over all flow.   But in streamwise component, the viscoelas-tic $\omega^+{}_{x,rms}$ decreases in comparison with Newtonian flow.   Fig. 10 shows the deficiency in the intensity of the streamwise vorticity fluctuations made dimensionless with u_τ/h against y^+ in the wall region to observe clearly.   The streamwise voticity
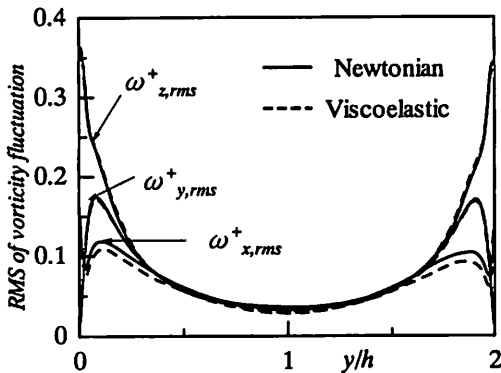

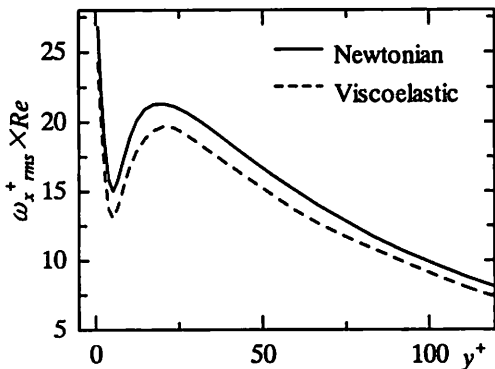Fig. 9   Root-mean-square of vorticity fluctuation vs y/h

Fig. 10   Root-mean-square of streamwise vor-ticity fluctuation vs y^+

fluctuations for both the Newtonian and the vis-coelastic flows attain their local minimums at about $y^+\approx5$ and then attain their local maximums near $y^+\approx20$ (no location shift is shown in this computed results).   It was explained that, this behavior is under of the influence of streamwise vortices in the wall region.   It has been reasoned that[7], the locations of the local maximum corre-sponds to the average locations of the center of the streamwise vortices and the local minimum corre-sponds to the average locations of the edge of the streamwise vortices in the wall region.   The signif-icant intensity reduction in viscoelastic flow at the region between the local minimum to the local maximum implies a reduction in the intensity of the wall eddies[14].   The inhibition of near-wall eddies may hamper the turbulence production and be proposed as a possible mechanism of drag reduc-tion in the viscoelastic flow.

Sureshkumar et al.[14] introduced a measure of extension $\dot{E}$ to consider the term representing the vortex stretching/squeezing mechanism, because it was connected as the production with vorticity and suggested as an possible inhibition of drag reduc-tion mechanism.   We evaluate the extension of vorcity using analogous equation given by

$$\dot{E}(y)=\frac{\|\boldsymbol{D}\cdot\omega\|}{\|\omega\|} \tag{33}$$

Where $\|\omega\|=\Sigma\omega_i{}^2$ denotes the norm of an arbitrary vector $\boldsymbol{\omega}$. $\dot{E}$ is evaluated in average values and its profile is shown in Fig. 11 as function of y^+. As shown, in the case of the viscoelastic flow, the measure of extension is reduced partially in the buffer layer comparing to Newtonian flow. It means a lower vortex stretching is existed when polymer molecule is introduced to the Newtonian flow.

6.5 Correlation of velocity fluctuation and streak spacing

The correlation coefficient of the streamwise velocity fluctuation at two-points separated in the spanwise direction is computed by
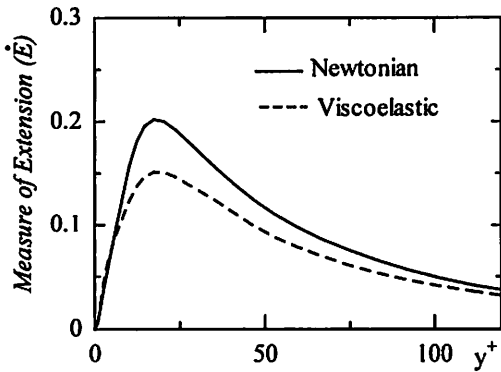
Fig. 11　The measure of extension

$$R_{uu}(\Delta z,y)=\frac{\langle u'(x,y,z,t)\cdot u'(x,y,z+\Delta z,t)\rangle}{\langle u'(x,y,z,t)\cdot u'(x,y,z,t)\rangle} \quad (34)$$

This correlation profile is illustrated in Fig. 12 at $y^+=10.24$ plane in buffer layer as a function of spanwise spacing $\Delta z^+(\Delta z^+=\Delta z u_\tau/\nu)$. For both of the Newtonian and viscoelastic flows, the correlation coefficients start with a maximum at $\Delta z^+=0$ and then become negative and reach a minimum. The locations at which this minimum occurred provides an estimate of the mean separation between the high and low speed fluid, and mean spacing between the streaks in the buffer layer should be roughly evaluated as twice of the distance between spanwise spacing of maximum and minimum location[7]. As presented in Fig. 12, the streak spacing for Newtonian flow is about 108.6
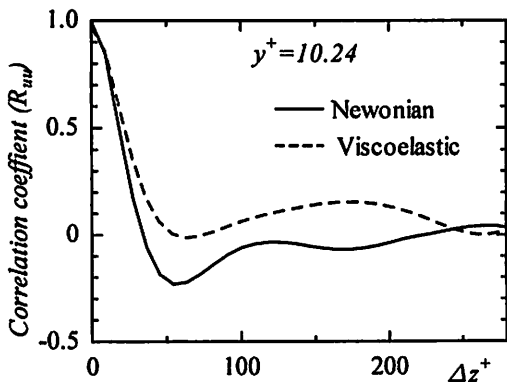
$(\Delta z^+\approx54.3)$ while the streak spacing of viscoelastic flow is about 128 $(\Delta z^+\approx64)$. It indicates the introduction of the polymer conducts the increasing in streak spacing. This is also in qualitatively good agreement with the database of experiments.

6.6　Measure of the molecule extension

The eigenvalue of the average conformation tensor, trace (C) is sought as a measure of the molecular extension, since it expresses the deformation of the molecules represented in the FENE-P model and in turn gives rise to the polymer shear stress contribution. The trace (C) profile obtained in fully developed viscoelastic turbulent flow is presented in Fig. 13 as a function of y^+. As we can see from here, the molecular extension is much higher near the wall $y^+\leq10$ and then monotonically decreases towards the channel center line. It implies that, the extension flow near the wall plays a important role in drag reduction. This is because an extensional flow is suitable to leading high molecular extension and thus leading to extensional viscosity.

7.　Conclusions

In this work, we successfully developed the high-order accuracy finite difference method to the viscoelastic turbulent channel flow, by using the dumbbell FENE-P model simulating the polymer chains. The several characteristics have been evaluated and the polymer additive effects obser-
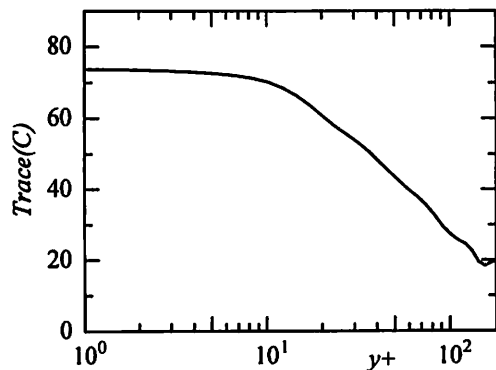

Fig. 12　Span correlation of streamwise velocity fluctuation

Fig. 13　The trace of conformation tensor C

ved experimentally have been realized and captured numerically. By comparing between the Newtonian and viscoelastic flows, the following points have become clear.

1) In the viscoelastic turbulent flow, we obtained the results of that, the upward shift of mean velocity profile in the logarithmic region, enhanced streamwise velocity fluctuation with decreased wall-normal/spanwise velocity fluctuations, decreased Reynolds shear stress, and increased streak spacing. All of these effects are in good qualitative agreement with the results obtained by the measurements and computations in the previous investigations.

2) The intensity of the streamwise vorticity fluctuation within the buffer layer is suppressed in viscoelastic flow. The extension of this vorticity fluctuation also shows a lower activity in the buffer layer. Nevertheless, the molecular extension measured as the trace of conformation tensor is attained a larger value near the wall. The connection between drag reduction and extensional properties might be proposed from here.

3) It has been demonstrated that, the high-order accuracy finite difference method could be applied for the viscoelastic flow by using FENE-P model without an artifficial diffusive term. The advantage of the computational scheme we used here is more remarkable in applications to viscoelastic flow simulations in complex flow geometry than spectrum method did.

References

1) Virk, P. S. et al., The Toms phenomenon : turbulent pipe flow of dilute polymer solutions, J. Fluid Mech., (1967), vol. 30, pp. 305-328.

2) Wei, T. and Willmarth, W. W., Modifying turbulent structure with drag-reducing polymer additives in turbulent channel flows, J. Fluid Mech., (1992), vol. 245, pp. 619-641.

3) Rudd, M. J., Velocity measurements made with a laser dopplermeter on the turbulent pipe flow of dilute polymer solution, J. Fluid

Mech. (1972), vol. 51, pp. 673-685.

4) Luchik, T. S. and Tiederman, W. G., Turbulent structure in low-concentration drag-reducing channel flows, J. Fluid Mech. (1988), vol. 190, pp. 241-263.

5) Walker, D. T. and Tiederman, W. G., Turbulent structure in a channel flow with polymer injection at the wall, J. Fluid Mech. (1990), vol. 210, pp. 377-403.

6) Bird, R. B. et al., Dynamics of Polymeric Fluids, vol. 1, (1987), Wiley, New York.

7) Kim, J. et al., Turbulence statistics in fully developed channel flow at low Reynolds number, J. Fluid Mech. (1987), vol. 177, pp. 133-166.

8) Wedgewood, L. and Bird, R. B., From Molecular Models to the Solution of Flow Problems, Ind. Eng. Chem. Res. (1988), vol. 27, pp. 1313-1320.

9) Den Toonder, J. M. J. et al., Drag reduction by polymer additives in a turbulent pipe flow : numerical and laboratory experiments, J. Fluid Mech. (1997), vol. 337, pp. 193-231.

10) Kajishima, T. and Miyake, Y., Drag Reduction by Polymer Additives in Turbulent Channel Flow Simulated by Discrete-Element Models, Trans. JSME, B (1998), vol. 64-627, pp. 110-117. In Japanese.

11) Bird, R. B. et al., Dynamics of Polymeric Liquids, vol. 2, (2nd ed.), (1987), John Wiley & Sons.

12) Massah, H. et al., Added stresses because of the presence of FENE-P bead-spring chains in a random velocity field, J. Fluid Mech. (1997), vol. 337, pp. 67-101.

13) Chiba, K. et al., The Society of Rheology, Japan (1999), vol. 27, pp. 31-42, In Japanese.

14) Sureshkumar, R. et al., Direct numerical simulation of the turbulent channel flow of a polymer solution, Phys. Fluids (1997), vol. 9-3, pp. 743-755.

15) Matsuzaki, K. et al., A Study on Numerical Analysis Method of Incompressible Flows Using High-Order Accuracy Finite Difference Method, Trnas. JSME, B (1998), vol. 64-627, pp. 4-10, In Japanese.

16) Peterlin, A. Streaming Birefringence of Soft Linear Macromolecules with Finite Chain Length, Polymer (1961), vol. 2, pp. 257-264.

17) Nakamura, K. Non-Newtonian Fluid Mechanics, (1997), CARONA publishing Co., LTD., In Japanese.

18) Kim, J. and Moin, P., Application of a Fractional-Step Method to Incompressible Navier -Stokes Equations, J. of Computational Physics (1985), vol. 59, pp. 308-323.

19) Rai, M. M. and Moin, P., Direct Simulations of Turbulent Flow Using Finite-Difference Schemes, J of Computational Physiscs, (1991), vol. 96, pp. 15-53.

20) Kawamura, T. and Kuwahara, K., Direct Simulation of a Turbulent Inner Flow by Finite-Difference Method, AIAA-85-0376, (1985), pp. 1-10.